Growth of Small Alumina Clusters during Ladle Deoxidation

Mats Söder, Pär Jönsson and Lage Jonsson

Division of Applied Process Metallurgy, Department of Materials Science and Engineering, KTH, SE-100 44 Stockholm, Sweden

(Received October 23, 2009)

ABSTRACT

For the first time, the size distribution of small clusters was determined in a systematic manner from samples taken during deoxidation with aluminium in an induction-stirred ladle. Chemical and microscopic analyses of samples were performed. The results indicated rapid cluster growth throughout the experiment and at the end of the experiment a majority of the small inclusions were found to be bound in clusters. The cluster growth was concluded to be by collision. Growth-model calculations were carried out to verify the experimental findings. In order to perform these calculations, a method first needed to be developed for conversion of the experimental data determined per unit area to data given per unit volume. Next, the cluster collision diameter was modelled using a theory for fractal aggregates. The results from the growth-model calculations, simulating deoxidation with aluminium, were found to agree well with the experimental results.

Keywords: Deoxidation, Alumina clusters, Growth, Collisions, Inclusions, Ladle

1. INTRODUCTION

Deoxidation is an important unit operation in secondary metallurgy. Because of the high demand today for steel grades of low oxygen content, deoxidation with aluminium has become a standard procedure. Aluminium is chosen since it is a strong deoxidant and relatively inexpensive. The deoxidation product, alumina inclusions, are solid oxides. By collision, the inclusions grow in a branched, loose manner and become clusters.

Much work has been done to mathematically describe the deoxidation process. Lindborg and Torsell /1/ conducted ground-breaking work and mathematically described a laboratory deoxidation experiment which used silicon as a deoxidant. Inclusion growth due to collision promoted by buoyancy differences (Stokes) and turbulent gradients (Saffmann and Turner) was modelled. As the formed silica is liquid, the radius of the collision product, r_k, was set to $r_k = (r_i^3+r_j^3)^{1/3}$ in their model.

Since then several researchers have also modelled deoxidation with aluminium. Models of ladles /2-5/, RH-degassers /6, 7/, and tundishes /7-9/ exist. A common characteristic of the different models is that the *size of growth products* is calculated according to the Lindborg and Torsells /1/ model that used silicon. The branched, more voluminous, cluster behaviour of alumina is therefore mostly not taken into account. In some models /7, 9/, however, it has been considered in modelling the flotation of clusters. In one previous case, a tundish model by Tozawa et al. /10/, inclusion growth which considered cluster size based on the theory of fractal aggregates was calculated.

Commonly when the subject of clusters is dealt with in the literature, it is with respect to very large clusters, which often appear late in the steel production process (usually in tundishes and during casting). This study, however, focused on the growth of inclusions and formation of initial small clusters through examination of samples taken during the initial ten minutes of a deoxidation experiment in an induction-stirred plant ladle. The experimental procedure employed is described in the following section of the report. Next, the counting or tallying of inclusions and clusters on the examined polished samples with an optical microscope and the importance of using the appropriate magnification (found to be 500x) is presented. For the counting, a technique based on a modification of the Swedish standard SS 11 11 16 /11/ was used. The composition of the steel samples was determined, specifically the aluminium and total-oxygen contents, and from these data the dissolved oxygen content was calculated. Later, growth calculations were carried out, in which the decrease in the calculated dissolved oxygen content was partly used as input data to the model. The oxygen bound to inclusions was calculated as the difference between total and dissolved oxygen and was compared with oxygen found in inclusions from the microscopic examination.

Information on inclusion and cluster growth has been of interest to the steelmaking community for a long time, as mentioned earlier, and is the reason the study included calculations of growth by turbulent collision. In order to calculate cluster growth, it was necessary to know the size of the cluster, i.e. collision area. Equations based on a theory for fractal aggregates were therefore formulated. The model predictions were then compared with the results from the microscopic examination of the samples. Note that in order to compare the growth-calculation results with the microscopic results, conversion of the experimental data from number per area to number per volume was required. This was a highly complex task and was at this point only developed to consider t2 clusters on the sample plane. Finally, four collision-growth calculations based on different assumptions were performed and the results compared to the experimental findings.

2. EXPERIMENTAL PROCEDURE

A full-scale experiment was carried out at the ladle furnace station at Ovako Steel AB's steel plant in Hofors, Sweden. The mill is a scrap-based special steel mill, where about 100 tonnes of scrap is melted in an electric arc furnace (EAF). The molten steel is tapped into the ladle and transferred to the slag removal unit, where the EAF slag is removed by raking. Thereafter, the ladle is transferred to the ASEA-SKF ladle furnace station, where aluminium for deoxidation, other alloys and synthetic slag are added. After the initial ladle treatment, the steel is vacuum degassed in order to remove, for example, sulphur and hydrogen. Finally, some additional stirring is carried out to promote inclusion removal before the steel is cast using up-hill teaming. The final bearing-steel product usually contains an average total oxygen amount of 5 ppm /12/.

2.2 Plant Trials

The full-scale experiment was conducted during the initial ladle treatment. Aluminium bars placed on the bottom of the empty ladle were used for pre-deoxidation. After tapping of the steel from the electric arc furnace, the remaining EAF slag was first thoroughly removed at the slag raking station. New synthetic slag was then added and melted at the ladle furnace. Thereafter, the ladle was moved to a nearby location where the experiment was carried out. This point in time is equal to the initial time in the deoxidation process when the ladle has just arrived at the ladle furnace. Upwards stirring by induction at 1000 A was used during the whole sampling procedure. Sampling was started with an initial sample in order to obtain a reference value. Thereafter aluminium wire (Ø 15 mm) was fed into the steel. A separate wire feeder than the one used in regular operation was used due to the special experimental location. In total, about 65 kg aluminium (~130 m) was fed into the steel during the experiment. During feeding of the aluminium wire, four samples were taken. After the aluminium wire feeding, two more samples were taken. Thus, in total there were seven sampling. The sampling protocol for the experiment is given in **Table 1** below.

Table 1
Sampling Protocol.

Time	Activity	Al (m)/(kg)
0.00	First sampling before Al feeding	0/0
2.03	Sampling	42.9/21.5
3.37	Sampling	73.7/36.9
4.29	Al feeding stopped due to problem with feeding	
4.44	Al feeding started again	
5.09	Sampling	98.1/49
6.42	Sampling	
7.03	Al stopped	129.9/65
8.16	Sampling	
9.47	Sampling	

2.2 Sampling Equipment

The samples were taken with an automatic sampler at a position 0.6 m below the steel surface and a little bit beyond the centre, as viewed from the inductive stirrer. A Rescon disc-pin type of sampler, model DP8 1100/900 /13/, was used. This is a specially designed sampler with an extra long splash protection shield covering the paper tube. The sample mould was protected from slag and steel inlet during immersion by purging argon gas through the mould. At the right sampling depth, the gas was switched off and the mould was filled by suction. This procedure ensured that the steel sample was taken at the targeted position.

2.3 Chemical Analysis Methods

Total oxygen content was determined using the inert-gas fusion method with a Ströhlein ON-MAT 8500. Each sample was analysed two times. The lower of the two values obtained was chosen to represent the total oxygen content. Chemical composition was determined by optical emission spectroscopy with a Bausch & Lomb ARL OES 3560 instrument.

3. SIZE DISTRIBUTION

A microscope is the primary instrument employed for determining the amount of inclusions in a steel for quality classification and production control. As the microscopic methods using standards like ASTME45 /14/, Stahl Eisen's standard SEP 1570-71 /15/ and SS 11 11 16 /11/, have been developed for finished steel products they are adapted to deformed steels. During deformation, alumina clusters break up and form elongated strings, which are characterised by length and width. For the undeformed steel samples taken from the ladle in this study, a different method to describe their surface representation was necessary to use. It should be noted that observed clusters on the sample surface are seen as random plane cuts through three-dimensional structures. The number of inclusions visible in an identified cluster is therefore not necessarily the total number that actually comprises the cluster. This will be further discussed later in the paper.

3.1 Inclusion Counting Method

Before any counting could be performed, the samples were carefully ground and polished. After this, an area of 400 mm^2 on the samples was examined with a light optical microscope (LOM) at 500x magnification. Individual inclusions were assessed using the Swedish standard SS 11 11 16 (JK Scale II) method /11/. Clusters observed on the surface were classified by the number and size of the inclusions of which they were comprised.

For the round type of inclusions (i.e. "undeformable inclusions, D type") that are of interest here, the SS 11 11 16 method /11/ classifies size by thin (T), medium (M), heavy (H) and particular (P). According to the standard, the sizes are "instrument dependent". In this investigation, the size ranges used were 1.7-3.5 µm, 3.5-6.9 µm, 6.9-13.8 µm and >13.8 µm. However, for inclusions in clusters, inclusions smaller than 1.7 µm were counted and the smallest size was 1 µm. The number of inclusions in a visual field is described in the SS 11 11 16 standard with an index, x, that gives the number of inclusions according to 2^{x-1}. For example the code T3 means that four T inclusions are observed in the visual field. For clusters a different notation was

used. Individual clusters were instead classified by *observed* inclusion sizes and number of inclusions. For example, the code M1T4 indicates that the cluster is made up of one M and four T inclusions. For clusters, the microscope employed was equipped with a digital camera and pictures were taken of some selected clusters.

3.2 The Role of Magnification in Viewing Clusters

The magnification used in examining the samples was 500x, though 200x is more commonly used in the SS 11 11 16 method. The difference between 200x and 500x magnification can be seen in **Figure 1**. At 200x magnification in the left picture (a), the cluster appears to contain two inclusions. When magnification is increased to 500x (picture b), the cluster instead is observed as containing four inclusions on the surface. Thus, it is important to view inclusions using different magnification in order to get a more complete description of the clusters.

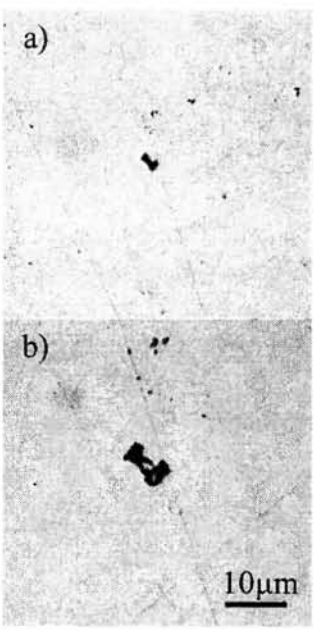

Fig. 1: Cluster viewed at 200x (a) and 500x(b) magnification.

3.3 Cluster Evolution during Deoxidation

Using the modified counting technique, the number inclusions and clusters were counted using the microscope. An increase in the number and size of clusters as a function of process time could easily be observed. There was a great increase in these numbers from the sample taken before the aluminium wire addition to the first sample taken after the start of deoxidation. At this early stage, the increase in the number of small clusters was substantial. Later, as the deoxidation experiment proceeded, the increase in the number of inclusions included in the clusters was pronounced. In **Figure 2** some pictures illustrating the cluster growth are presented.

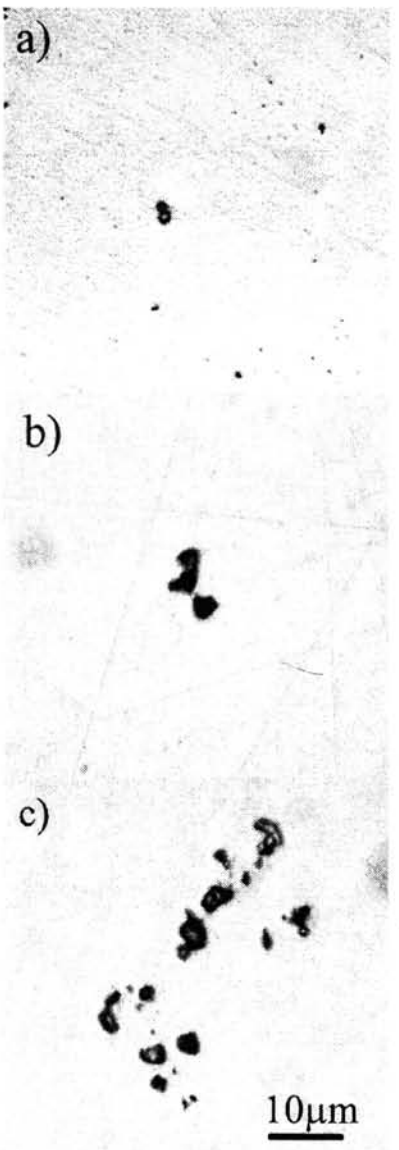

Fig. 2: Clusters of different sizes seen on the surface of a polished steel sample. Photo a) t2-cluster, b) t4 cluster and c) t11 cluster.

Note that the clusters seen on the surface can easily contain more inclusions since the cluster is not two, but three dimensional. The number of inclusions in a cluster is presented as the number 'observed on the sample surface' (2D).

There was a significant increase in the number of inclusions when the aluminium feeding began. The number of single small t inclusions increased almost threefold and t2 clusters more than fivefold. This increase is plotted in **Figure 3**. In order to make a comprehensible presentation of this information, the number of inclusions of size T, t2, t3 and t4 is presented as the number observed. Clusters containing more inclusions than four were summed up and presented in the >t4 group. It can be seen that single inclusions (T) first increase rapidly when the Al feeding is initiated. This can be expected since many inclusions are formed when the dissolved oxygen content decreases (further discussed in section 4). Also, an increase in the number of all small clusters can be observed during the whole experiment. Noteworthy, is the relatively rapid increase in the amount of clusters larger than t4 after the stop of aluminium addition (the two last sampling time points).

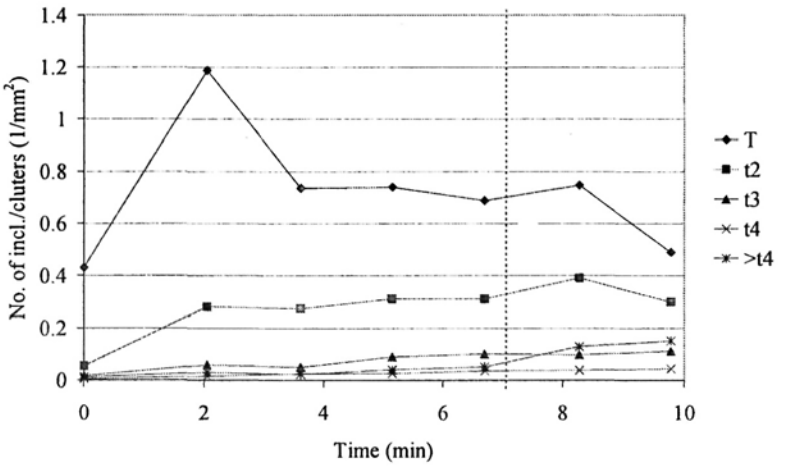

Fig. 3: No. of single small inclusions (T) and small clusters as function of time. Numbers determined with microscope. Dotted vertical line indicates end of aluminium addition (start at time zero)

Here, it is important to note that the diameter of a cluster influences the likelihood of it being observed on the sample surface. This relationship between number of inclusions of a certain size in the steel volume N_V, and the number visible on the surface N_A, can be better understood by studying **Equation 1** /16/, where the diameter is taken to be the external diameter of the cluster, D_e, i.e. the diameter of a sphere that surrounds the whole cluster. If the number of clusters in two size groups increase and the relation between them per unit volume stays the same, the number of clusters in the surface will increase for the larger sized as the quotient between the diameters of the clusters in the larger and the smaller size group.

$$N_V = \frac{N_A}{D_e} \qquad (1)$$

The single T inclusions and t2 clusters seem to be connected to the aluminium feeding as they increase in number during feeding and thereafter decrease at the time point of the last sampling. During the deoxidation process there is a shift towards larger size clusters. In **Figure 4** it can be seen that the percentage of t2 clusters decreases in relation to the total amount of clusters during and after the aluminium feeding. When the aluminium feeding is stopped, the relative number of inclusions bound to clusters containing five or more inclusions increases. Similarly, Feng /17/ observed in laboratory deoxidation experiments an increase in the size of clusters.

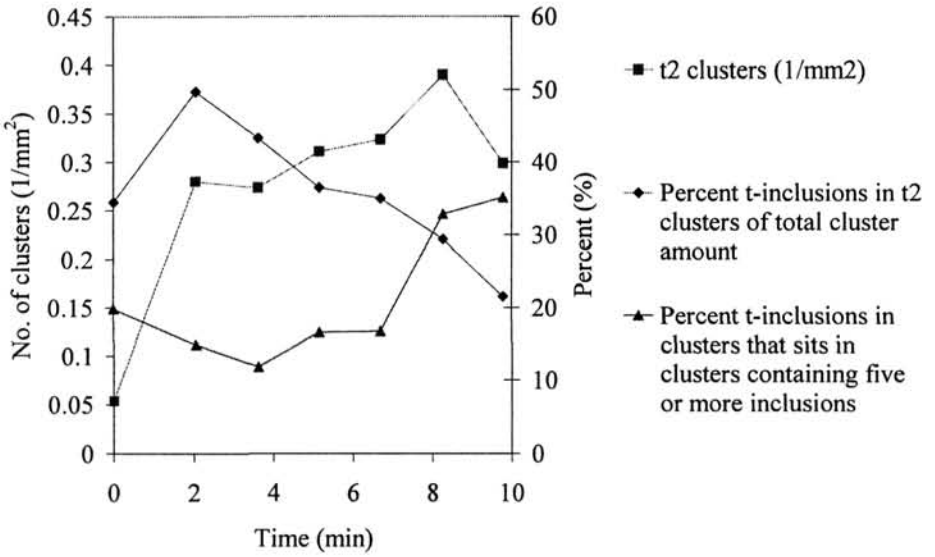

Fig. 4: No. of t2 clusters and percentage t inclusions in clusters compared to total cluster amount.

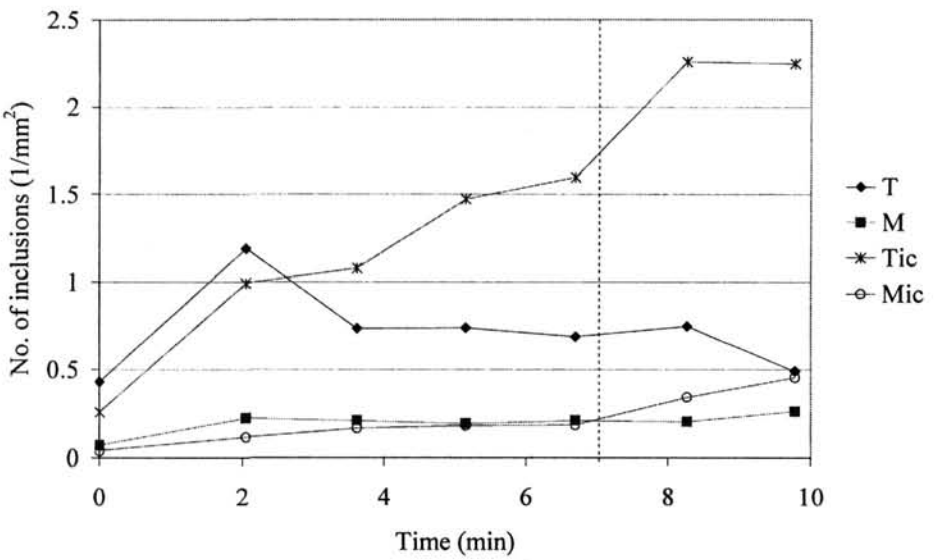

Fig. 5: Number of inclusions bound and unbound to clusters. T and M denote the single inclusions of size T (1.7-3.5 μm) and M (3.5-7 μm). Tic and Mic are the number of T- and M-size inclusions bound to a cluster.

The number of inclusions bound to a cluster increased significantly throughout the experiment. In **Figure 5** this is quite clear for T-size inclusions and can also be seen as the case for M-size inclusions. Interestingly the increase in cluster-bound T inclusions (Tic) seems to stop after aluminium feeding ceases. At the same time, the number of single T inclusions decreases. These two observations can be interpreted as effects of the collision growth of inclusions in the steel.

4. ALUMINIUM AND TOTAL OXYGEN CONTENTS

The amount of alumina inclusions that are formed during deoxidation is controlled by the amount of aluminium and oxygen in the steel. These amounts are thereby connected to the number of inclusions and clusters that can be found on a sample surface. The dissolved oxygen amount was calculated using a mass

balance between aluminium and total-oxygen concentrations determined by chemical analysis. The amount of oxygen bound to inclusions calculated as the difference between total and dissolved oxygen was compared with the amount of oxygen calculated based on inclusions from the microscopic examination. Later, in the growth-model calculations, the decrease in the dissolved oxygen content was partly used as input data to the model.

As previously mentioned, the steel was first deoxidised upon tapping of the electric arc furnace with aluminium bars placed on the bottom of the empty ladle. The added aluminium resulted in a total aluminium content of 0.007 % by weight at the start of the experiment (**Figure 6**). Thereafter, a total of 65 kg aluminium wire was fed into the steel for seven minutes, which resulted in a total aluminium content of 0.057 %. This corresponds to an aluminium yield of 77 %.

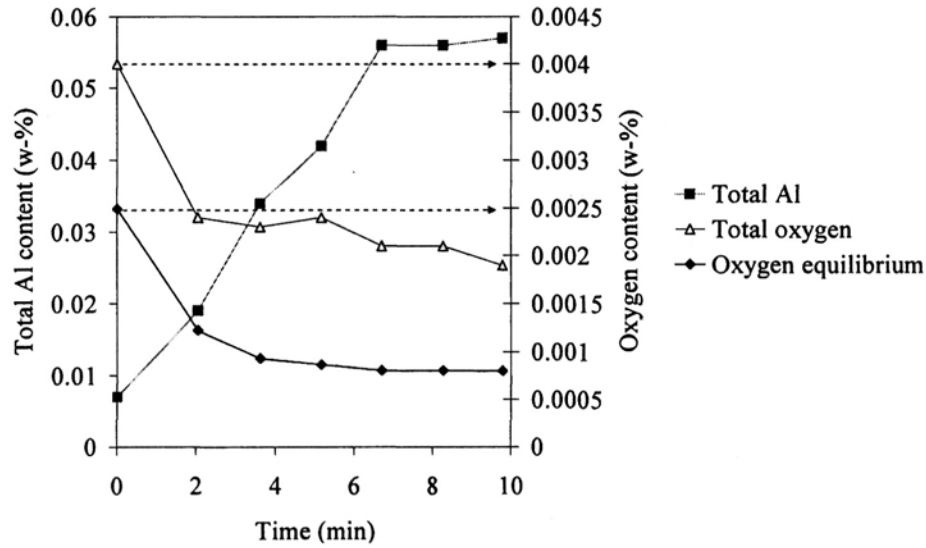

Fig. 6: Total aluminium and oxygen contents determined from chemical analysis and calculated dissolved oxygen content plotted as a function of time (% by weight). Plotted total oxygen content is lowest of two values determined from each sample.

One effect of the deoxidation is seen in plotting the results for total oxygen content. As shown in **Figure 6**, the oxygen content is initially 40 ppm, a result of the first deoxidation upon tapping of the EAF. The total oxygen then drops to 19 ppm at the end of the aluminium-wire feeding. This value corresponds very well to the average total oxygen value of 19 ppm reported by Huet et al. /12/ for samples taken three minutes after the end of aluminium feeding at Ovako Steel AB. Thus, the experimental heat is representative of normal production conditions.

The dissolved oxygen content was calculated using the following equation:

$$2\underline{Al} + 3\underline{O} = Al_2O_3\,(s) \qquad (2)$$

$$\Delta G^\circ = -1202050 + 386.3T\ (J/mol)\ /18/ \qquad (3)$$

The activity of oxygen and aluminium was calculated based on the interaction with elements in the steel. The element concentrations are provided in **Table 2**. The interaction parameters were taken from Elliott et al. /19/. The dissolved aluminium content was iteratively calculated from the determined total aluminium content to balance with the dissolved oxygen content. A dilute-solution approximation was used in the calculations, where the activity of alumina was assumed to be one and the steel temperature was assumed to be 1600°C.

Table 2

Steel Chemical Composition (percent by weight)

C	Si	Mn	Cr	Mo	Ti
0.61	0.28	0.27	0.41	0.03	0.0008

An observation in **Figure 6** that clearly stands out is the initial rapid drop in total oxygen. This corresponds to a rapid removal of alumina deoxidation products from the steel. Calculated as alumina, the oxygen drop is equivalent to 3.4 kg for the whole ladle - or as seen on a surface: 12.8/mm^2 as 3 µm inclusions. The mechanism behind this initial inclusion removal is not fully known by the authors but some possible explanations are suggested later in the report.

The oxygen amount that is equal to the difference between the determined total oxygen content and calculated dissolved oxygen content is bound to inclusions. This bound oxygen amount is seen as inclusions on the polished samples. This means that it can be calculated from the observed fraction of inclusions on a sample surface. The amount of bound oxygen was calculated using **Equation 4** for the samples taken in the study and compared with the difference between the determined total oxygen content and calculated dissolved oxygen content in **Figure 7**.

$$O_{Al_2O_3} = \frac{M_{OmAl_2O_3} \cdot \rho_{Al_2O_3} \cdot F_{incl}}{M_{Al_2O_3} \cdot \rho_{Fe}} \quad (4)$$

where $M_{OmAl2O3}$ is the molar weight of oxygen in alumina, ρ_{Al2O3} is the density of alumina (3990 g/m^3) /20/, F_{incl} is the area fraction of inclusions, M_{Al2O3} is the molar weight of alumina and ρ_{Fe} is the steel density (7100 kg/m^3) /20/.

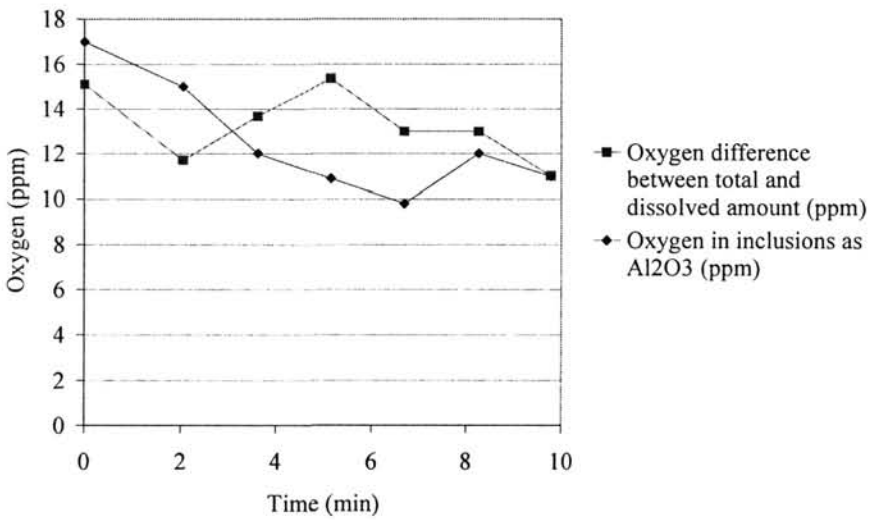

Fig. 7: Difference between total oxygen and dissolved oxygen amounts shown in Fig. 6 compared with oxygen amount calculated to be contained in Al_2O_3 inclusions.

The curve for the calculated oxygen in inclusions (as Al_2O_3) shows quite good agreement with the difference between total and dissolved oxygen. The trends are declining in both curves although not so pronounced for the difference between total and dissolved oxygen. The curve for the calculated oxygen amount in inclusions should lie under the curve for the difference between total and dissolved oxygen as it is reasonable to believe that not all inclusions existing on a sample surface will be identified. This will be discussed further below.

It should also be noted that the calculated amount of oxygen in inclusions as alumina is based on the surface-area fraction. It is dependent on the size and number of inclusions. The very large inclusions of size P are defined by their specific size and individually substantially contribute to the area fraction. The percentage contribution to the area fraction from the different size classes is plotted in **Figure 8**. It can be seen that large P-type inclusions give a large contribution initially and this steadily decreases through the duration of the experiment. Further it is seen that the contribution from small inclusions increases during the aluminium feeding.

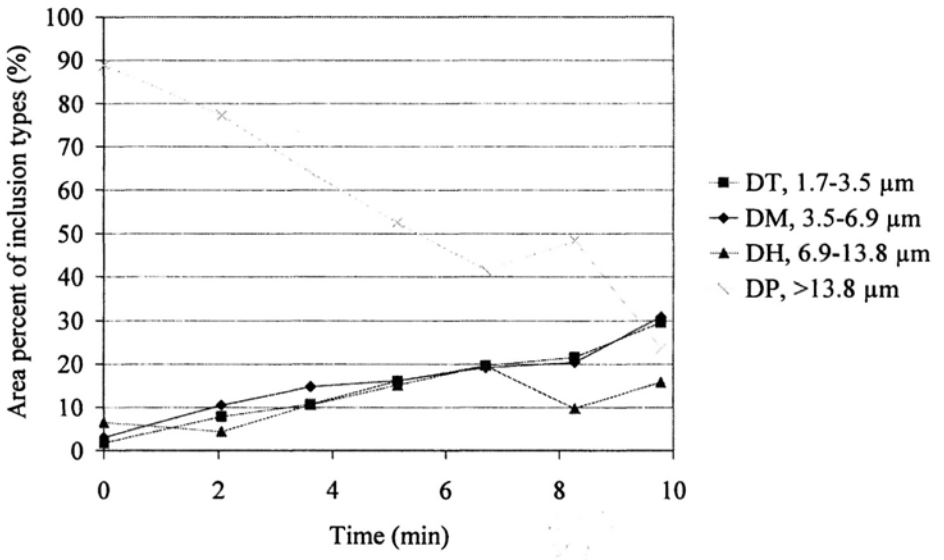

Fig. 8: Proportion of the different size classes to surface-area fraction of inclusions. Inclusions in clusters individually counted.

The calculated oxygen amount in inclusions is composition dependent. Composition affects the stoichiometric and the density of the oxides. In the microscope it was observed that many of the large P inclusions were perfectly round. This means that they were liquid and, based on the current experimental conditions, were most likely composed of a high amount of silicon oxides. Huet et al. /12/ reported that Al_2O_3-SiO_2-MnO *inclusions* of size 6 to 40 micrometers that originate from predeoxidation with FeSi are present during this part of ladle treatment. Silica inclusions would render a lower oxygen amount in the inclusions due to the low density of these inclusions. This would probably lead to the first part of the curve for the calculated oxygen amount in inclusions being under the curve for the difference between total and dissolved oxygen in **Figure 7** since the proportion of P inclusions in the area fraction is initially large **(Figure 8)**.

5. CALCULATION OF CLUSTER GROWTH

As mentioned in the introduction, many researchers have developed models of inclusion growth, but only a few have taken cluster growth into consideration in their calculations. In the results of the microscopic examination of samples in this study a clear increase in the amount and size of clusters in the studied part of the deoxidation period was seen. Thus, it is vital that this type of growth must be taken into account in any growth model for alumina inclusions. With this in mind, model calculations were performed in order to see if similar results to what was found in sample examination by microscope would be obtained. In order to do this, it was first necessary to determine cluster size regarding growth by collision. It was also essential to be able to convert the results from the microscopic analysis, which are determined in number per unit area, to number per unit volume as used in the calculations of the growth model.

5.1 Turbulent Growth

Due to the induction stirring of the steel in the ladle, the fluid flow is turbulent. The turbulence causes velocity gradients which give rise to collisions between the inclusions. The number of turbulent collisions may be calculated based on Saffman and Turners /21/ equation:

$$\frac{dn_{ij}}{dt} = 1{,}3\pi^{1/2}\alpha\left(r_i + r_j\right)^3\sqrt{\frac{\varepsilon}{\nu_{Fe}}}n_i n_j \qquad (5)$$

where α is the collision efficiency, r_i and r_j are the radii of the two colliding particles, ε is the local turbulent energy dissipation of the steel in the ladle and ν_{Fe} is the kinematic viscosity

5.2 Derivation of Cluster Size Model

In **Equation 5** the radii of the colliding particles affects the collision rate in a cubic relation. It is therefore necessary for accurate calculation of the collision growth of inclusions and clusters to know the geometrical relationship between the number of inclusions in a cluster and its size. It should also be noted that cluster-removal models developed in the future would need to consider the geometry of clusters. Removal was however not dealt with in this work.

5.2.1 Alumina Clusters as Fractal Aggregates

In nature and in industrial applications, fine particles and similar systems are known to form fractal aggregates[22]. Alumina inclusions in steel seem to be no exception. Some researchers have considered this when describing the behaviour of clusters /9, 10, 23/. In the theory of fractal aggregates the size-number relationship is:

$$N = k_e \left(\frac{R_e}{r_i} \right)^{Df} \tag{6}$$

where N is the number of inclusions, k_e is the power law prefactor or numerical density, R_e is the external radius, r_i is the inclusion radius and Df is the fractal dimension. The external radius, R_e, is the radius of a sphere that surrounds the whole cluster. The fractal dimension has a value between 1 and 3.

The number of inclusions in the cluster is described by the fractal dimension and the k_e prefactor. In the physical system, the number of inclusions is determined by the clustering behaviour of alumina inclusions. For example, the size of the individual inclusions, coordination numbers, deformability of formed cluster structure, sintering, collision mechanisms, etc. all affect the size-number relationship of a cluster. Thus, it is understood that clusters can have the same fractal dimension but different numbers of inclusions. When D_f is the same in the equation, the number of inclusions that comprise a cluster is determined by the prefactor *ke*. The prefactor then describes the number density of the cluster given a certain diameter.

5.2.2 External Diameter and Collision Area of Small Clusters

It is of vital importance in modelling growth by collision that the size of the clusters be known since the collision rate is dependent on the collision area. The size of clusters in the calculation is controlled by both the power-law prefactor, k_e, and the fractal dimension, *Df*.

In the work of Tozawa et al./10, 22/ it was concluded that the fractal dimension should have a value of 1.8. Note, that the fractal dimension has not been measured for alumina clusters. However, it seems reasonable that the fractal dimension would be approximately 1.8 since both simulations /24, 25/ and experiments /26-28/ with systems resembling the alumina system have produced values of around 1.8.

The actual size of the clusters should be derived from measurements of real clusters. For small clusters, which are the focus of this research, an expression for the external diameter was derived from the form of the t2 cluster. Setting the fractal dimension to 1.8, the prefactor k_e then becomes 0.57 for the case where the cluster inclusions are the same size (**Equation 6**). Based on the two-inclusion cluster case, and rearranging the equation for fractals, the external diameter can then be written as:

$$D_e = 2d_i \left(\frac{N}{2} \right)^{1/1.8} \tag{7}$$

However, this diameter cannot be used in a collision model since it would lead to overestimation of the cluster collision area. The degree of overestimation can be exemplified by the two-inclusion cluster case. In **Figure 9** the collision area is shown for two different cuts through the two-inclusion cluster. In the x , y and z directions, the dimension varies from d_i to $2d_i$. A collision diameter can then be defined using the average diameter in the three directions:

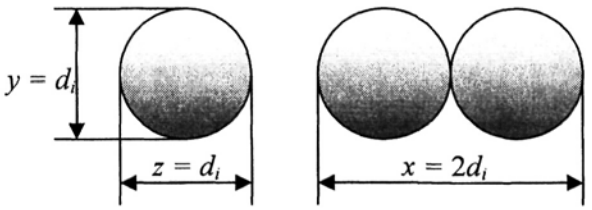

Fig. 9: The collision dimensions in the X, Y and Z directions.

$$D_c = \frac{x+y+z}{3} = \frac{2+1+1}{3} d_i = \frac{4}{3} d_i \qquad (8)$$

This diameter can subsequently be used to formulate an expression for the collision diameter:

$$D_c = \frac{4}{3} d_i \left(\frac{N}{2}\right)^{1/18} \qquad (9)$$

The k_e prefactor for this case is equal to 1.19 when N = 2 and $R_e = {}^4/_3 r_i$ in **Equation 6**.

A comparison was made in order to examine how the theoretically derived diameters D_e and D_c correspond to actual observation of cluster sizes. Some clusters were photographed, as illustrated earlier in **Figure 2**. This was done mainly for the largest clusters, but for the sake of completeness, also for a few small ones. Thereafter, the external diameter, D_e, was measured and the number of inclusions, n_A, was counted from these pictures. The number of inclusions in a cluster seen on the polished surface was then recalculated to the number of inclusions in the whole cluster as follows:

$$N = \frac{2 n_A D_e}{3 d_i} \qquad (10)$$

The equation uses the relation between the number of inclusions on a surface and in the volume similar to what was presented in **Equation 1**. The number of inclusions in a cluster is determined based on the cluster area and the volume defined by the cluster diameter, D_e. It is also assumed in using the equation that i) the inclusions are of the same size, ii) the cluster is cut through the centre, and iii) the inclusion number density seen on the surface is the same for the entire cluster.

In **Figure 10** is the recalculated number of inclusions in the cluster plotted as a function of the observed external diameter. It can be seen that for the smaller clusters, the number of inclusions is higher than the line for the external diameter plotted using **Equation 7**. The equation for the collision diameter, Dc, describes the size of the small clusters better. However, the number of inclusions for the small clusters is most likely somewhat overestimated as their shape is more two dimensional. The values determined for larger clusters lie between the two lines.

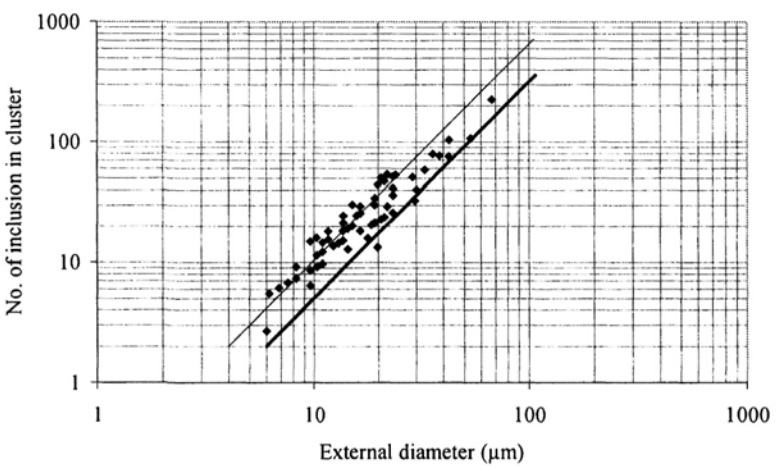

Fig. 10: Number of inclusions seen in cluster on polished sample surface converted to number of inclusions in 3D derived from $N_V = N_A/d_i$ relationship. Upper line defined by D_c and lower (bold) by D_e.

5.3 Conversion of Data Per Unit Area To Data Per Unit Volume

Up to this point in the report, determination of cluster size distribution discussed has been based on results from counting what could actually be observed on the two dimensional sample surfaces (section 3.1). However, these results from sample examination by microscope cannot be used directly as starting values in a growth model, as they are given in number per square mm ($1/mm^2$). They need to be converted to number per unit volume ($1/m^3$). In addition, the surface representation of clusters must be considered. This section presents how a derivation of the surface representation of t2 clusters can be done and how convertion of the data given per unit volume can be performed. It should be noted that a clear understanding of surface representation of clusters is vital when making comparisons between growth-model results and microscope results.

5.3.1 Probability of Observing Small T2 Clusters

When determining the size distribution of alumina inclusions on a polished steel sample by microscope, some errors arise due to the fact that the cuts through the inclusions are rarely made precisely through the centre of the inclusions. As a result, a "false" diameter will be seen as illustrated in **Figure 11**. This is a known problem and can be compensated for as suggested by, for example, Underwood[16].

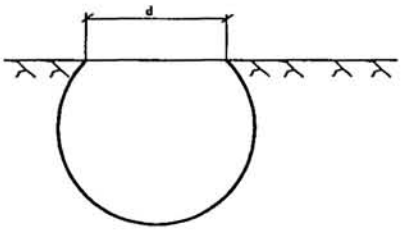

Fig. 11: A "false" diameter viewed on the surface of a polished steel sample.

When it comes to counting alumina inclusions that have collided before the steel solidified, i.e. formed clusters, the problem is further complicated because not all clusters on the surface appear as clusters. Thus, in order to obtain more realistic numbers of the size distribution of clusters in a sample based on information from microscopic assessment, a more reliable method of determining *cluster* size distribution *had* to be developed. In the following text, the developed method for converting the two-dimensional information ($1/mm^2$) to three-dimensional ($1/mm^3$) for the case where a cluster contains two inclusions is presented.

The fact that not all clusters in the surface are seen as clusters is illustrated in **Figure 12** for clusters made up of two inclusions, here called t2 clusters.

Fig. 12: Clusters containing two inclusions on surface of polished steel sample. Note that sample surface must be ground down to grey area (a) for the t2 cluster to be seen.

If the cluster in **Figure 12a** is to be viewable as a t2 cluster in a plane cut, the sample must be ground down to the grey area. Note that the height of the grey area is a little bit less than the inclusion overlap in the grinding direction since there is a minimum size of inclusions that can be seen through a microscope. If a conversion from number of t2 clusters seen on the surface to number of t2 clusters per unit volume is to be made, it is absolutely necessary to know the proportion of t2 clusters that should be visible on the surface. The probability that an observed cluster is a t2 cluster is calculated below in converting a number actually seen

on a sample (per mm^2) to a corresponding number per volume (per mm^3). In doing this, the following assumptions were made:

1. The inclusions are spherical
2. The two inclusions in the t2 cluster have the same radius length
3. The inclusions are randomly orientated in the steel matrix
4. There is a minimum diameter that can be seen with the microscope

The validity of these assumptions is discussed later in the report.

By studying one inclusion as a sphere and assuming that a connected inclusion of the same size can sit on the sphere at any position, the average angle to the surface of the polished sample can be determined to have a value of 30°. This angle is illustrated in **Figure 13**. At a 30° angle, the distance in the z direction of one of the inclusions is equivalent to half the radius length. This average contact point is located as indicated by the dashed line where the area A1 equals A2 on the half-sphere of the lower inclusion.

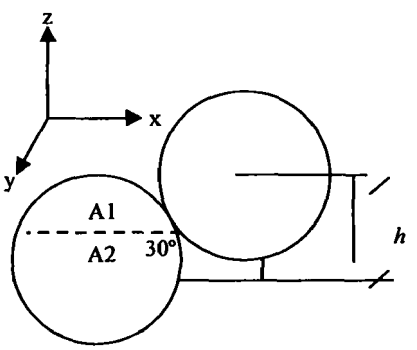

Fig. 13: Average angle t2-cluster radii form with sample surface.

The likelihood that both inclusions of a t2 cluster on the surface have been cut through can be calculated from the geometric relationship illustrated in **Figure 13** between the height h and total height (P_{t2} = 1/3). The probability that only one of the inclusions in the t2 cluster has been cut can also be calculated from the figure (P_{t1} = 2/3). This can also quite easily be simulated or substantiated by making an integration calculation. However, here it is of interest to convert the results of what is actually seen on the surface to what can be found in a volume (2D to 3D or $1/mm^2$ to $1/mm^3$) and vice versa. As there is a minimum diameter for when an inclusion can clearly be observed, a reliable convertion should take a visible diameter into consideration. Furthermore it should be related to a certain depth in order to relate what is seen on the surface to what is under the surface. The likelihood of seeing a t2 cluster on the surface with the microscope was here defined as equivalent to the quotient of two sums. The first sum represents the sum of all heights, h_v, at all positions on a sphere that gives a visual t2 cluster for all angles (δ_v). The second sum is the sum of the total height, h_{tot}, (or depth if related to the polished surface) equal to a circum-ambient diameter of the t2 cluster, i.e. here $4r$ and (later called D_e) for all positions around the sphere. The number of connection positions for the inclusions at a certain angle is related to the circumference of the sphere, C, perpendicular to the z axis. The summation is done by integrating the product of the heights and the circumference with respect to the angle, δ. The nomenclature and geometric relationships used in the derivation are defined in **Figure 14**.

As mentioned above, the angle of the t2 cluster must be large enough to produce a segment diameter for both inclusions that is greater than the smallest viewable diameter ($2a$). This angle, δ_v, can be expressed as

$$\delta_v = \arcsin(a/r)\delta \tag{11}$$

It was estimated that the smallest diameter that can be seen with the microscope is 1 μm in length and the average size of a T inclusion is 3 μm. For this case the δ_v angle is 20°. The smallest possible δ_v value is taken into account in the derivation below.

As seen in **Figure 14**, the height h_v can be expressed as:

$$h_v = 2l - 2r\cos\delta = 2\sqrt{r^2 - a^2} - 2r\cos\delta \tag{12}$$

and the circumference at the contact point perpendicular to the z axis is

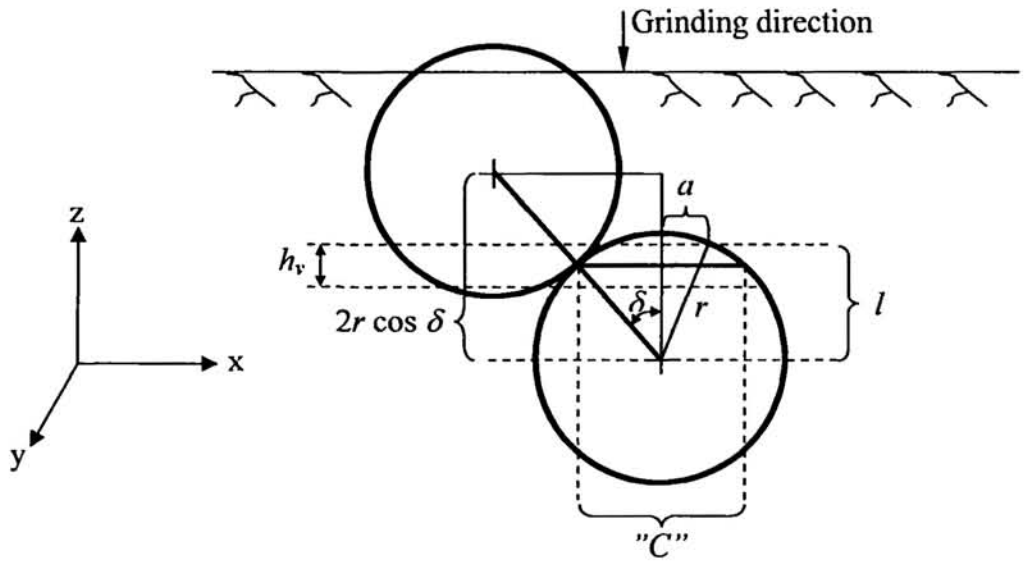

Fig. 14: Relationships used in calculating probability that a t2 cluster will be visible.

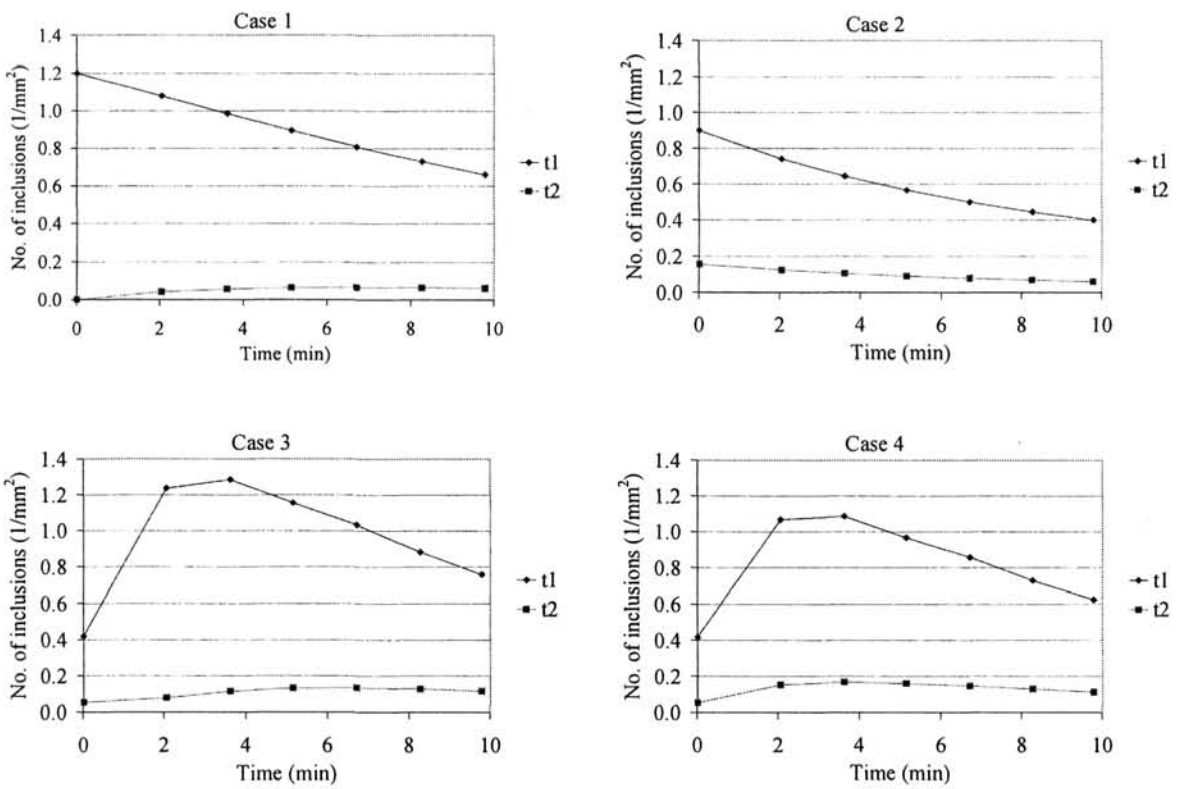

Fig. 15: Model calculations, cases 1-4.

$$C = 2\pi r \sin\delta \tag{13}$$

Thus, the following integral is obtained:

$$\int_{\delta_v}^{\pi/2} 4\pi r\sqrt{r^2 - a^2}\sin\delta - 4\pi r^2\cos\delta\sin\delta d\delta = \left[-4\pi r\sqrt{r^2 - a^2}\cos\delta + \pi r^2\cos 2\delta\right]_{\delta_v}^{\pi/2} \tag{14}$$

Similarly for the total height, the following expression can be formed:

$$\int_0^{\pi/2} 8\pi r^2\sin\delta d\delta = \left[-8\pi r^2\cos\delta\right]_0^{\pi/2} \tag{15}$$

which leads to the following expression of probability:

$$P_{t2} = \frac{\left[-4\pi r\sqrt{r^2 - a^2}\cos\delta + \pi r^2\cos 2\delta\right]_{\delta_v}^{\pi/2}}{\left[-8\pi r^2\cos\delta\right]_0^{\pi/2}} \tag{16}$$

For a viewable diameter ($2a$) of 1µm and an inclusion size of 3µm, the chance of seeing a t2 cluster as a t2 cluster is 0.22, or 22%. This probability is represented by the case seen in **Figure 12b**.

Similarly, the probability of seeing the t2 cluster as a single T inclusion is 0.50, calculated with:

$$P_{t1} = \frac{\left[-8\pi r\sqrt{r^2 - a^2}\cos\delta\right]_0^{\delta_v} + \left[-2\pi r^2\cos 2\delta\right]_{\delta_v}^{\pi/2}}{\left[-8\pi r^2\cos\delta\right]_0^{\pi/2}} \tag{17}$$

However, single inclusions were counted strictly according to the SS 11 11 16 standard and the smallest inclusions counted were 1.7 µm. Using this diameter and thus setting a to 0.85 reduces the probability to 0.48.This is represented by the case seen in **Figure 12c**.

The likelihood that a t2 cluster is not visible at all, i.e. that it lies at a depth of 4r, corresponds to the remaining 30%. Some inclusions that are not visible have been cut such that their diameter is less than the smallest viewable diameter. Others are simply not cut at all. The former case is illustrated by **Figure 12d** and the latter by **Figure 12e**.

5.3.2 Conversion from 2D to 3D

Knowing the probability of how the t2 clusters are represented in the surface is not enough for the sought after conversion of data given per area to data given per volume. Thus, an equation using the number of inclusions, size and probability was needed.

Conversion of the information determined from the two-dimensional sample surface to data expressed per unit volume for spherical inclusions is a standard procedure for those who work with data from microscopic analysis. It can be done using the following relationship /16/:

$$N_V = \frac{N_A}{d_i} \tag{18}$$

where N_V is the number of inclusions per unit volume, N_A is the number of clusters per unit area, and d_i is the inclusion diameter. For t2 clusters the equation is:

$$N_V = \frac{N_A}{P_{t2}2d_t} \text{ or } N_V = \frac{N_A}{P_{t2}D_e} \tag{19}$$

For larger clusters the theoretical representation in a sample surface is much more complicated than for t2 clusters. As the inclusions grow larger they extend in all directions in a random manner. Cuts through this random structure will show it to be comprised of fewer inclusions than it actually is. Some may even be seen as t2 clusters in the surface. The proportion of larger clusters taken to be t2 clusters, based on what can be observed on a surface, is unknown. The task of determining this is significantly more complex and requires a greater amount of knowledge on the stochastic geometrical form of clusters and thus was beyond the scope of this study.

5.4 Growth Calculations

In order to find out if the increase in the number of clusters as seen by microscope could be predicted with the growth model presented in **Equation 5**, four

calculations were made. The populations of inclusions/clusters from t1 to t20 were calculated. However, due to the uncertainty of how to estimate the number of multi-inclusion clusters in a surface, only t1 and t2 inclusions were plotted for comparison with the microscopic results. Note that only growth was considered and the removal of inclusions was thus neglected. This will, of course, need to be considered in a future more extensive study on the growth and removal of small clusters during deoxidation.

In the calculations it was assumed that the collision efficiency was 0.3, the energy dissipation was 0.01 m^2/s^3, the viscosity was 0.005 kg/sm and the single inclusion size was 3 μm. Furthermore, the radius of clusters containing a certain number of inclusions was set according to the collision diameter, D_c (**Equation 9**). Inclusions were added or subtracted according to the collision rate considering the population balance. Cluster size in calculating the number of clusters per mm^2, N_A, was set as the external diameter, D_e. The conversion from N_A to the number of t2 clusters per unit volume, N_V, and vice versa was done using **Equation 19**.

For the initial values and presentation in 2D ($1/mm^2$), the probabilities as described in section 5.3 were used. As single inclusions were strictly counted according to the SS 11 11 16 method, the smallest inclusions counted were 1.7 μm. This meant that for 3 μm inclusions, only 82% of the inclusions on the surface would be counted (calculated $(1.5^2-0.85^2)^{1/2}/1.5$). In the growth calculation this probability was considered.

In order to show how different assumptions and input data influence predictions on cluster growth, four separate calculations are presented. First, two simple calculations were done in order to show how only growth without any aluminium addition during the stirring influences the growth predictions:

Case 1: Starting with a total number of inclusions of $1.2/mm^2$ evenly distributed as 3 μm single inclusions. The initial value $1.2/mm^2$ was chosen based on the number of single T inclusions found in **Figure 3**. The alumina content was assumed to be constant.

Case 2: Starting with a total number of inclusions of $1.2/mm^2$ and assuming inclusion size to be 3 μm. The inclusions were assumed to initially be distributed as t1 and t2 inclusions in accordance with the microscope results for the first sample. The alumina content was assumed to be constant.

As cases 1 and 2 do not consider the aluminium addition in the experiment, they will not reflect what was seen in the results of the production experiment. In the microscopic analysis results, presented in **Figure 3**, it can be seen that the number of inclusions increases rapidly in the first sample after aluminium wire feeding. Simultaneously, the total oxygen content and calculated dissolved oxygen content decreased rapidly, which is illustrated in **Figure 6**. The formation of small inclusions and the drop in dissolved oxygen content are most likely related to each other. Assuming that the formed alumina is reflected in the drop in dissolved oxygen content, this decrease could be used as input to the growth calculation. However, the amount of alumina formed in relation to the drop in dissolved oxygen is much greater than what is seen as the increase in small inclusions in the microscope on the samples. Also in **Figure 6**, the decrease in total oxygen corresponds to a removal of oxygen in alumina inclusions (this is discussed further later). The amount of oxygen bound in oxide (the difference between total and dissolved oxygen) seems however more or less constant over time and not related to what is seen to be occurring with the population of small inclusions. It is for these reasons not correct to directly use the drop in dissolved oxygen. Instead, it was found that 11% of the decrease in dissolved oxygen corresponded to an increase in small 3 μm inclusions.

Based on the above discussion, two more calculations were done using the data pertaining to the decrease in dissolved oxygen:

Case 3: Starting with the same amount of t1 and t2 inclusions as detected by microscope on the surface of the first initial sample (**Figure 3**), then calculated with an addition of alumina as the amount of "formed alumina" corresponding to 11% of the decrease in dissolved oxygen content (**Figure 6**).

The alumina was distributed as t1 inclusions and the values updated at each sampling occasion.

Case 4: Similar to case 3, but alumina was distributed between t1 and t2 inclusions as the distribution seen on the first sample (**Figure 3**).

In **Figure 15** the results from the different calculations are shown.

The calculations show that t1 inclusions decrease in number quite a lot – by about one third - due to growth into larger inclusions. Also, the number of t2 clusters tends to decrease if there are not enough t1 inclusions or "added" t2 clusters to compensate for the loss due to collision growth.

It is obvious that the calculations where all alumina was added initially, cases 1 and 2, do not render results that show agreement with the microscope results in **Figure 3**. This is because they do not consider the continuous addition of the deoxidants. It is, however, interesting to note that the number of t2 clusters does not increase in case 2. In case 1, the amount of t2 clusters increases and, although hard to see in the figure, starts to decrease at the end of the calculation. In cases 3 and 4, the number of t2 inclusions eventually begins to decrease because the number of t1 inclusions that can grow to become t2 inclusions is not high enough. Instead, the decrease in t2 inclusions due to collision growth has a greater effect on the final number of t2 inclusions.

The predictions for case 4, where an addition of t2 clusters due to aluminium feeding is included, show the best agreement with the results from microscopic analysis in **Figure 3**. More specifically, the predicted peak value is almost 1.1/mm^2 for the t1 inclusions. This is a slightly lower value than the experimental value of 1.2/mm^2, which is taken from the microscopic results in **Figure 3**. However, the agreement between predicted and experimental data is quite good.

The experimental values from the microscopic study pertaining to t2 inclusions are higher than the predicted values in **Figure 14**. One possible reason for the deviation is that some of the larger inclusions on a sample surface can be cut such that they are actually seen as t2 inclusions. Also, smaller clusters, for example t3 - t12, that are present in greater numbers than larger clusters, would have a higher chance of being cut such that they are mistaken for two-inclusion clusters. The actual probability of this in numerical terms is not known to the authors and would be an appropriate subject for future research. However, to get an idea regarding what effect this might have on a more realistic prediction, the number of t2 clusters was modified to incorporate the assumed influence of the number of t3-t12 clusters on the number of t2 clusters. In **Figure 16**, half of the t3-t4, one third of the t5-t6, one fourth of the t7-t8, one fifth of the t9-t10 and one sixth of the t11-t12 clusters were added to the number of t2 clusters. It can be seen that the predicted change in the t2 cluster population with stirring time agrees much better with the results in **Figure 3** when those additional assumptions were made. This indicates that any future investigation aimed at better prediction of the evolution of t2 clusters with stirring time needs to include the influence of clusters consisting of more than two inclusions on the probability of finding a t2 inclusion on a surface.

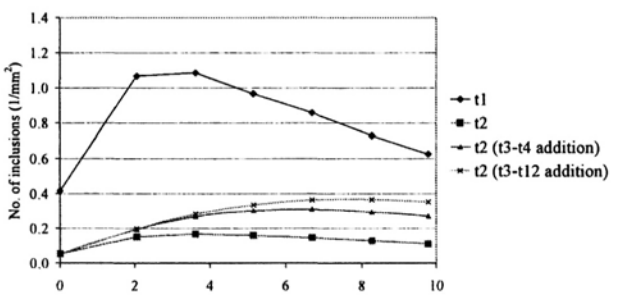

Fig. 16: Calculation case 4: results modified with assumed t2 addition from the number of t3-t12 clusters.

In **Figure 15,** showing the cluster-growth calculation results for the four cases, only t1 and t2 clusters are shown since these can be more accurately presented as seen on a polished surface and therefore be compared with the microscopic examination results. As a comparison, the predicted values for the clusters per unit volume from calculation case 4 are plotted in **Figure 17**. Interestingly enough, the curves for t3, t4 and >t4 clusters resemble the ones seen in **Figure 6** of the microscopic results although they have a bit higher values here. It is also worth noting how the group

representing clusters made up of at least four inclusions (>t4) increases with stirring time. First, while there are few smaller clusters, the increase is small. Later, when smaller clusters – the "bricks" that large clusters are made up of - have formed, the growth rate increases.

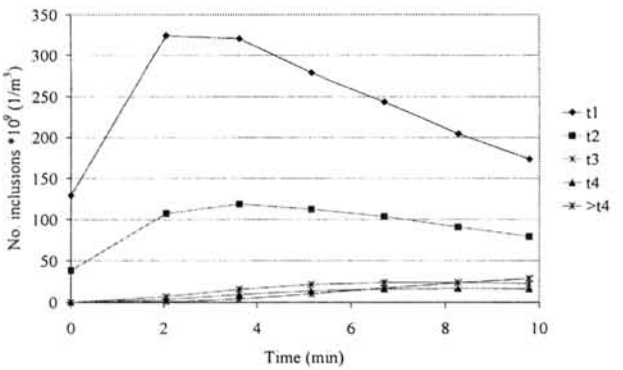

Fig. 17: Results of model calculation case 4 with no. of inclusions per unit volume.

6. DISCUSSION

6.1 Cluster Size Distribution

There seems to be no contribution from secondary alumina inclusions (due to the decrease in oxygen solubility upon solidification of the sample) to the size distribution of inclusions in the steel. Especially, the initial sample (before Al wire addition) should be used as a reference and compared with the other samples. Although the dissolved oxygen content is much higher in the first sample, the numbers of inclusions seen on the sample surface in the microscopic analysis are much fewer. If secondary alumina inclusions would exist, they would be expected to be present as small inclusions which would be formed from the oxygen dissolved in the steel. Also, the use of 500x magnification should have exposed any significant contribution of secondary inclusions. Thus, it is most likely that any formed secondary alumina inclusions may therefore be expected to be substantially smaller than 1 μm. Another indication that no contribution of secondary inclusions to the size distribution of inclusions existed, is the calculation results of the oxygen amount found in inclusions in the microscopic examination, **Figures 7** and **8**. These calculations show good agreement in the difference between the total oxygen content and the dissolved oxygen content.

The microscopic results in **Figure 3** show that alumina inclusions form clusters during deoxidation. It should be noted that the observed clusters are mostly made up of two, three and four alumina inclusions. Thus, these clusters are very small compared to what has previously been discussed regarding clusters in the open literature. These small clusters are present during the entire 10-minute deoxidation experiment. The larger clusters (three or more inclusions per cluster) increase in number and size throughout the deoxidation experiment. It should be noted that the increase, especially for the t4-clusters, continues after the stop of aluminium addition after 7 minutes. This is taken as evidence that cluster formation/growth is due to collisions in the steel bulk and not primarily a result of aluminium addition.

As implied by the proposed theory for determining the probability of actually seeing a t2-cluster on the surface of a steel sample, far from all clusters are seen in their true nature. This is because they are three dimensional and can be oriented and cut in any direction. The number of larger clusters will for this reason be underestimated. Thus, in reality, a number of observed t2 clusters on a sample will actually be larger clusters. The proportion of larger clusters mistaken for t2 clusters is not known by the authors at this time, but it seems likely that for example t3 and t4 clusters would appear as t2 clusters than t3 and t4 clusters on the sample surface.

As the single inclusions grow to form small clusters they decrease in number as observed on the sample surface. Simultaneously, the number of large clusters increases. Growth of clusters may therefore be wrongly interpreted as removal if microscopic examination is performed at 200x magnification. It is thus important to count all inclusions in the clusters to get the full picture. The amount of removed inclusions in this investigation does not seem to be very high. The cluster growth is though much more obvious.

6.2 Aluminium and Oxygen Equilibrium

The loss of aluminium during wire feeding is much larger than what corresponds to the decrease in the

oxygen content determined by chemical analysis (**Figure 6**). The loss is therefore not due to rapid deoxidation and removal of deoxidation products. Instead, it is more reasonable to believe that due to the slow feeding speed some of the aluminium is burnt off at the surface of the ladle or in the slag. The loss, corrected for the removed alumina, is estimated to correspond to a 0.8 mm rind around the 15 mm wire.

The total oxygen analysis results show a drastic decrease after the start of aluminium addition. This would represent a very fast removal of oxygen through alumina inclusions. This could be explained if the oxygen is removed by the formation of very large inclusions that have very high buoyancy that almost float directly up to the surface. The fluid flow towards the surface could also assist in the transport of these large inclusions. No increase in very large inclusions was observed in any of the samples that were examined by microscope. However, if the inclusions were about 100μm or larger they would be so rare that it is unlikely that even one such inclusion would have been observed on the examined surface. Another, maybe more far-reaching explanation might be the precipitation of inclusions directly to the ladle wall and top slag. It was earlier calculated that the rapid drop in total oxygen corresponds to 3.4 kg alumina. If this amount was evenly distributed on the inside of the ladle, a 45 μm layer would form.

6.3 Clusters Growth

In the derivation of the conversion of number of t2 inclusions seen on a surface to number per volume, four assumptions were made. A few of these assumptions are, of course, a simplification of what really occurs in order to make calculation possible. The first assumption, that the inclusions are spherical, is not totally correct for alumina as the inclusions are solid in the steel and have a shape formed by crystallisation factors. However, the shapes of the majority of the observed small alumina inclusions are quite well extended in all three dimensions. Thus, the assumption of a spherical shape in the calculations can be seen as fairly good. Assumption number two, that the two inclusions forming a cluster are of the same size, is a generalisation that stands for the most. However, some minor errors in the calculations must result from applying this assumption. Assumption numbers three and four, that the inclusions are randomly oriented in the steel matrix and that there is a minimum diameter that can be seen in the microscope, respectively, can both be considered correct based on the observations in this study. In addition to these possible sources of error, there will also be some larger inclusions/clusters that are cut such that their visible diameter can be small and in the T size range. Their proportion in the number of observed inclusions/clusters depends on the size distribution of the single inclusions and is further complicated by the random cuts through clusters containing more inclusions than two.

As the extent to which larger clusters can be mistaken for observed t2 clusters on a sample surface is not known, the accuracy of the latter part of the curve in **Figure 3** from the microscopic examination is therefore somewhat questionable regarding what inclusions and clusters were actually seen on the surface. This especially makes any comparison between single t1 inclusions and t2 clusters using the probability of seeing small t2 clusters a bit unsure for this part of the curve. However, the initial values pertaining to the early part of the deoxidation are less affected by collision growth and considered less likely to be influenced by the presence of larger clusters. For the initial values in the growth calculations, this would have a minor effect, but it was neglected in this work.

Depending on what starting data is used in the calculations, very different results were obtained. It was found that a method for taking the aluminium addition into consideration is necessary for more accurate modelling. The calculations also showed that the alumina addition both in amount and what size, in terms of number of individual inclusions in the clusters, has a clear affect on the modelling results. A conclusion drawn when comparing the growth calculations for cases 3 and 4, is that the high ratio between t2 and t1 inclusions can not be explained by the collisions of single t1 inclusions. In case 4, there is an increase from formed alumina being distributed both to t1 and t2 inclusions. Thus, a greater resemblance to the t2 curve in **Figure 3** from the microscopic examination is obtained. This implies that clusters are not only formed

by collision in the steel bulk but also directly at the spot of alumina addition, if the growth calculations are to be considered fully accurate. There may thus be different growth rates and even growth mechanisms for inclusions in the vicinity of the addition spot and the rest of the steel bulk.

At the same time as the calculated dissolved oxygen decreases very rapidly, it was observed from the microscopic sample analysis that there is a large increase in the number of small inclusions. In cases 3 and 4 of the growth model calculations, the rate of the drop in dissolved oxygen content was used as the rate of formation of new inclusions. It was shown that the growth could be modelled based on this assumption. This result could be of interest for a process-control model for inclusion behaviour in stirred melts since it is based on relatively easily measurable and attainable values. As inclusions collide and clusters grow continuously in the stirred steel bath, a growth model should also consider the "age" of the melt after deoxidation. Furthermore in developing a deoxidation model, it appears vital to know the initial oxygen content of the steel melt at the start of deoxidation.

Inclusion removal was not considered in the growth calculations. However, from the microscopic analysis results, no obvious effect of removal on the inclusion population could be observed. As the dominant mechanism for removal is generally considered to be flotation of inclusions to the top slag, which is very much controlled by the buoyancy, the increase in buoyancy for the small clusters formed could be too minor to have any pronounced effect on the inclusion population. It should also be noted that the buoyancy of clusters has by several researchers /7, 9, 10/ been regarded to be limited by the increased density of the clusters; thinking of the fluid dynamics, the steel is "locked" in the structure of the cluster.

It seems readily apparent that the fractal form of alumina clusters requires further investigation. It is reasonable to believe that the fractal dimension for different steel qualities and different operational lines is the same, around 1.8. The numerical density value, k_e, may though vary some depending on chemical composition, size of the individual inclusions, the lapse of time after the aluminium addition and other physical parameters. For accurate modelling of the removal characteristics, it would be of great value to understand the flotation process of alumina clusters. It would thus be necessary to investigate the D_f, k_e and actual effective inter-particle locking of steel (i.e. cluster density in the steel).

7. CONCLUSION

Inclusion growth and cluster formation have been investigated through examination of samples taken during a ten-minute deoxidation experiment in an induction-stirred plant ladle. Inclusions and clusters on polished samples were counted when viewed by microscope. Clusters were found in all samples and they were very small in comparison to what is normally reported in the open literature. Based on aluminium and total oxygen contents determined from chemical analysis, the amount of corresponding dissolved oxygen was calculated and the amount of oxygen bound in inclusions was compared with the microscopic examination results. In order to make a cluster growth model, a size equation based on the theory of fractal aggregates was developed and values determined applying the theory compared with the microscopic results. Four growth model calculations based on turbulent collision were performed. For comparison with the microscopic examination results, a method was developed for converting model data from numbers per area to numbers per volume for randomly oriented clusters containing two inclusions.

The primary findings of this investigation are the following:

1. Examining polished steel sample surfaces by microscope requires a level of magnification that allows inclusions present on the surface to be viewable as separate entities. A magnification of 500x provided the degree of resolution deemed necessary in this study.
2. The results from both the microscopic examination and the determination of aluminium/oxygen contents by chemical analysis indicated that most of the alumina inclusions are formed within the first two

minutes. The microscopic examination results showed a significant increase in the number of inclusions and clusters at the beginning of the aluminium feeding. During the experiment there was a shift towards the formation of larger inclusions. It is obvious that there is quite a large amount of clusters in the steel during ladle refining and that a majority of the small inclusions are bound to clusters. It was further concluded that the cluster growth was due to collision.

3. Both the results from the microscopic sample analysis and growth calculations indicated that not only single inclusions, but also larger clusters, are formed at the point of aluminium addition. The higher concentration of both inclusions and aluminium may lead to higher growth rates for inclusions in the vicinity of the location where the aluminium is added than for those in the steel bulk flow.
4. In predicting growth by collision, the equation formulated to express the collision diameter for small clusters was found to render reliable results. Good agreement with the microscopic observations was found when 11% of the decreased dissolved oxygen content was calculated as an addition of 3 μm inclusions distributed as single inclusions and clusters containing two inclusions.
5. In applying equations formulated to convert data from number per surface area to number per volume for clusters containing two inclusions lying in the surface it was concluded that only 1/3 of the clusters are actually oriented such that they could be theoretically observed as two-inclusion clusters. Moreover, these clusters can be positioned in such a manner that 2/3 could theoretically be mistaken for single inclusions. It was also concluded that some larger clusters may wrongly be observed as clusters containing two inclusions.
6. Although inclusion removal was not taken into account in this study, any future cluster-removal model would need to consider cluster form and the steel that is in hydrodynamic aspect locked in the structure of the cluster (i.e. effective cluster density in the steel).

REFERENCES

1. U. Lindborg and K. Torssell, *Trans. Met. Soc. AIME*, **242**, 94 - 102 (1968).
2. K. Nakanishi and J. Szekely, *Trans. ISIJ*, **15**, 522-530 (1975).
3. M. Hallberg, *En matematisk modell för desoxidation av en omrörd stålsmälta*, Tech. lic. Royal Institute of Technology, ISBN 91-7170-949-2 (1996).
4. D.Y. Sheng, M. Söder, P. Jönsson and L. Jonsson, *Scand. J. Metall.*, **31**, 134-147 (2002).
5. M. Wakoh, K. Fuchigami, K. Endoh, N. Imamura, A. Kiyose, I. Sawada, *Scanmet I*, Luleå, Sweden, June, 267-274 (1999).
6. K. Shirabe and J. Szekely, *Trans. ISIJ*, **23**, 465-474 (1983).
7. Y. Miki, Y. Shimada, B.G. Thomas, A. Denisov, *I&SM, ISS*, **28**, 31-38 (1997).
8. A.K. Sinha and Y. Sahai, *ISIJ Int.*, 33, pp. 556-566 (1993).
9. Y. Miki and B.G. Thomas, *Materials Transactions B*, **30B**, 639-654 (1999).
10. H. Tozawa, Y. Kato, K Sorimachi and T. Nakanishi, *ISIJ Int.*, **39**, 426-434 (1999).
11. Svensk Standard SS111116. Steel – Method for Assessment of the Content of Non-metallic Inclusions. Swedish Institute for Standards, June, (1987), pp. 1-16.
12. L. Huet, P. Jönsson and F. Reinholdsson, *Steel Times Int.*, **11**, 47-50 (1997).
13. H. Hägglund, Rescon-ElectroNite, P.O. Box 35, SE-190 63 Örsundsbro, Sweden.
14. Steel – Determination of content of non-metallic inclusions – micrographic method using standard diagrams, International Standard ISO 4967- (E) (1979).
15. Mikroskopische prufung von edelstählen auf nichtmetallische einschlusse mit bildreihen, Stahl-Eisen-Prufblatt 1570, Verlag Stahleisen, Dusseldorf 1, postfach 8229.
16. R.T. DeHoff and F.N. Rhines, *Quantitative Microscopy*, McGRaw-Hill, New York, (1968).
17. Y. Feng, *A Kinetic Study on the Deoxidation of Liquid Steel by Silicon and Aluminium*, PhD Thesis,

Royal Institute of Technology, ISBN 91-7170-828-6 (1995).
18. G.K. Sigworth and J.F. Elliott, *Met. Sci.*, **8**, 298-310 (1974).
19. J.F. Elliott, M. Gleiser and V. Ramakrishna, *Thermochemistry for Steelmaking*, Addison-Wesley, London, **2**, 620 (1963).
20. K. Asano and T. Nakano, *Tetsu-to-Hagané*, **57**, 1943-1952 (1971).
21. P.G. Saffman and J.S. Turner, *J.Fluid Mch.*, **1**, 16-30 (1956).
22. J. Feder, Fractals, Plenum, New York, 33 (1988).
23. K. Tozawa, Y. Kato and T. Nakanishi, *CAMP-ISIJ*, **7**, 276 (1994).
24. P. Meakin, *Phys. Rev. Lett.*, **51**, 1119-1122 (1983).
25. M. Kolb, R. Botet, and R. Jullien, *Phys. Rev. Lett.*, **51**, 123-1128 (1983).
26. D.A. Weitz and M. Oliveira, *Phys. Rev. Lett.*, **52**, 1433-1436 (1984).
27. P. Dimon, S.K. Sinha, D.A. Weitz, C.R. Safinya, G.S. Smith, W.A. Varady and H.M. Lindsay, *Phys. Rev. Lett.*, **57**, 595-598 (1986).
28. J.E. Martin, J.P. Wilcoxon, D. Schaefer and J. Odinek, *Phys. Rev. A*, **41**, 4379-4391 (1990).